Pupil Shape and Chromatic Aberration Can Provide Spectral Discrimination for "Color Blind" Animals.

Alexander L. Stubbs[1] and Christopher W. Stubbs[2]

The only known mechanism for color vision requires spectrally diverse photoreceptor types (1). However color vision comes at a cost: a reduction in the signal to noise ratio in low light conditions and angular resolution in each spectral channel. Coleoid cephalopods (octopus, squid, cuttlefish) have a single photoreceptor type (2,3,4) and lack the ability to determine color by comparing detected photon intensity across multiple spectral channels. Nevertheless, cephalopods produce vividly colorful mating displays and use adaptive camouflage to accurately match the color of their natural surroundings. This presents a paradox - behaviors that imply an ability to determine color in organisms with a monochromatic visual system - that has long puzzled vision scientists and biologists (5,6,7). Here we propose a novel mechanism for spectral discrimination: the exploitation of chromatic aberration (the wavelength-dependence of focal length) by organisms with a single photoreceptor type. Through numerical modeling we show how chromatic aberration can yield useful chromatic information via the dependence of image acuity on accommodation. The peculiar off-axis slit and annular pupil shapes in these animals enhance this chromatic signature. This picture is consistent with existing data on cephalopod behavior and retinal morphology, and may have broader applicability in other species.

Many species of cuttlefish, squid, and octopus live in colorful marine habitats. These cephalopods rely primarily on camouflage to defend against predation. Octopus and cuttlefish actively control chromatophores to provide a high-fidelity color match to natural backgrounds under diverse illumination conditions (Fig. 1b, c). This has been validated by laboratory and field observations using color photography (8), in-situ spectrophotometry (9,10,11), and hyperspectral imaging (12).

Some cuttlefish and squid signal to conspecifics using vividly colorful displays (Fig. 1a). These chromatic signals are highly visible to predators with color vision. It is hard to imagine that natural selection would favor the evolution and maintenance of these displays if the chromatic information content were invisible to the cephalopods themselves.

[1] Museum of Vertebrate Zoology, Dept. of Integrative Biology, UC Berkeley, Berkeley CA 94720 USA.
[2] Departments of Physics and of Astronomy, Harvard University, Cambridge MA 02138 USA.

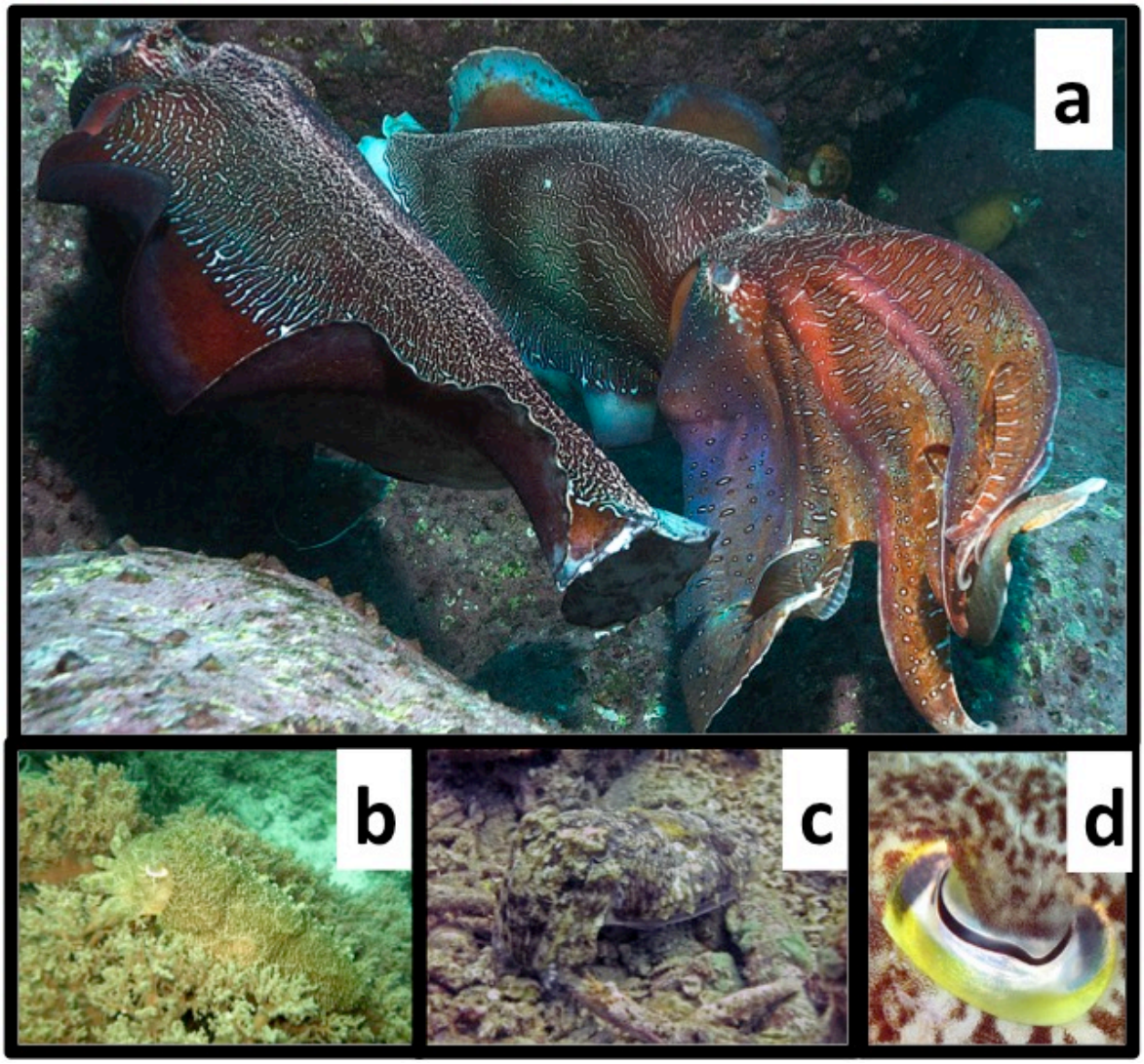

Figure 1. Cephalopod Behavior and Pupil Shapes. Many shallow-water cephalopods produce colorful displays (**a**, *Sepia apama*) to conspecifics, and accurately color-match natural environments to camouflage (**b**, **c** *Sepia latimanus*). How these animals accomplish this despite being "color blind" is a long-standing mystery. We propose that the variation of focal length with wavelength provides a mechanism for spectral discrimination. Their pupil shapes (**d** *Sepia latimanus*) maximize the chromatic aberration signature while minimizing other sources of image blur.

All but one cephalopod species studied possess (4) a single photoreceptor type, limiting them to a monochromatic view of the world. Despite early behavioral evidence indicating (13) color discrimination, more contemporary studies (2,3,4,5) produce results showing they lack multiple photoreceptor types. Previous attempts to reconcile this apparent paradox include suggestions that: (i) the animals do not change color but rather the brightness (or luminance) of their skin (14), (ii) color sensing could exist (15) in the skin of the animals, and (iii) undetected additional retinal photoreceptor types could allow for color vision (4). None of these potential

explanations has resolved the paradox and researchers continue to search for a mechanism that explains this seemingly "color blind camouflage" (5, 6, 7).

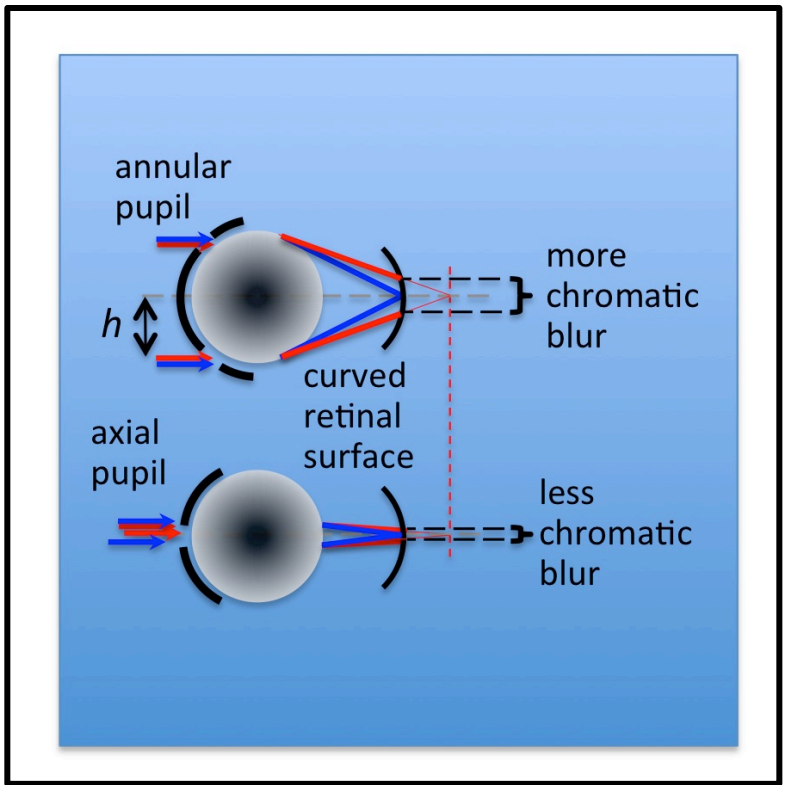

Figure 2. Chromatic Blur and Pupil Geometry. This illustration shows the two principles that underpin our proposed mechanism for color discrimination in a monochromatic visual system: (1) the chromatic shift in focal length for light of different wavelengths, and (2) the outermost ray's angle of incidence as it intercepts the optical axis determines the blur. The annular pupil produces more chromatic blurring than an on-axis pupil because it transmits rays with a larger ray height *h*.

The eye of *Octopus australis* has (16) a radial gradient in the index of refraction of the spherical lens, which (in conjunction with the index match between seawater, the lens edge, and the ocular fluid) produces images that are largely free from spherical aberration. However, the wavelength-dependence of the lens index induces (16) chromatic aberration, causing light of different wavelengths to have different focal lengths. When integrated over the wavelength dependence of the single cephalopod opsin response, this leads to chromatic blurring that dominates the image quality budget (Extended Data Table 1). Chromatic lens effects dominate over spherical aberration and other factors in a diversity of taxa.

Pupil shape plays a central role in determining the strength of chromatic blur (Fig. 2, Extended Data Fig. 2). While ambient light levels dictate pupil area, pupil shape determines chromatic blurring. Chromatic blur dominates the cephalopod image quality in low-light conditions, when the pupil is fully dilated. The off-axis slit and annular pupils these animals adopt in high-light conditions preserve this color

discrimination mechanism across a wide dynamic range of illumination. We conclude that natural selection in this system favors the maintenance of a chromatically aberrated image, and thus color discrimination wins out over image acuity. The annular pupil shape, (Fig. 1d) common in both cuttlefish and shallow-water squids, maximizes the off-axis distance of optical rays from objects in the horizontal plane around the animal. The horizontal slit pupil of shallow-water octopus species intercepts a similar ray bundle from objects on the ocean bottom, projecting an arc onto the upper portion of the retina that has an enhanced density of photoreceptors (17). This is accomplished at the expense of visual acuity, which would be maximized through an on-axis contracted pupil (Extended Data Fig. 2).

The central point of this paper is that the relationship between image acuity, spectral content, and the lens-to-retina spacing (18) provides a mechanism for spectral discrimination in creatures with monochromatic visual systems that are dominated (Extended Data Table 1) by chromatic blur (Figs. 2, 3). By finding the focal setting that produces the sharpest images, through accommodation, these animals can in fact determine the colors of objects with sufficient spatial structure.

We investigated the relationship between angular resolution, accommodation and spectral content. We conclude that the accommodation setting of best focus tracks (Fig. 3p,q) the spectral content of the scene.

Our proposed mechanism is a differential technique that requires sharp spatial intensity gradients combined with sharp spectral structure. This imposes limitations. Broad, overlapping spectral features are difficult to distinguish. Cephalopods would be unable to determine the spectral content of a flat field of uniform color, much as a photographer would also be unable to determine optimal focus for a uniform screen absent fine scale structure. Cephalopods would similarly be unable to determine spectral information from abutting regions of comparable apparent intensity, differing only in spectral content, because in that case the image sharpness is largely independent of accommodation (Fig. 3r). Natural environments are rich in shadows and structure that serve as focusing aids. We note that spectra measured (19) in marine environments frequently provide the sharp spectral features needed for this mechanism.

The intraspecific displays of these organisms (Fig. 1a) frequently exhibit black fine-scale structure abutting colored areas, facilitating contrast determination. This is another adaptation that favors our model.

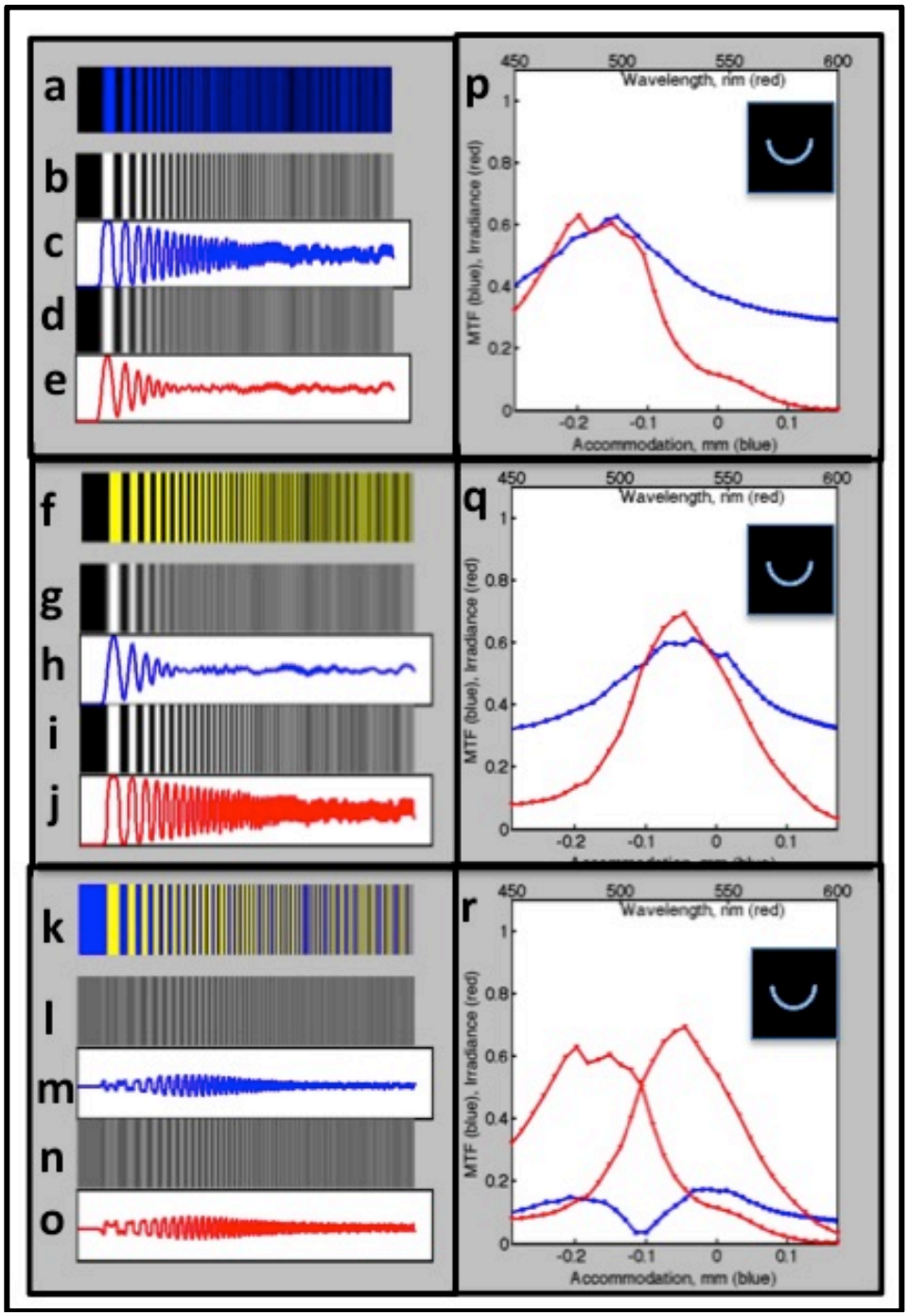

Figure 3. Chromatic Blur Simulations. Spectral information can be deduced from image sharpness vs. accommodation (lens-to-retina distance). Two-color bar chart test patterns (**a,f,k**) produce simulated chromatically blurred images at accommodation settings of -0.22 mm (**b,g,l**) and 0.00 mm (**d,i,n**) and corresponding line plots of intensity (**c,h,m** and **e,j,o** respectively). Accommodation settings of -0.22 mm and 0.00 mm correspond to best-focused wavelengths of 470 and 550 nm. The Modulation Transfer Function (MTF, blue in **p,q,r**) as a function of accommodation tracks the spectrum of detected photons (red in **p,q,r**). The inset shows the pupil shape used. The widest bright bar spans 165 microns on the retina.

Our simulations show a tremendous depth of field for objects beyond a certain range, when imaged at a single wavelength (Extended Data Fig. 4). This means that a scan through accommodation settings amounts to a spectral scan of the scene. For the lens we modeled, breaking range-color degeneracy occurs at ranges beyond the modest value of 1 meter. The sharpest image is achieved at an accommodation setting that depends exclusively on an object's color and not on its distance. What about when objects are closer than this? The accommodation setting needed to create a crisp focus of a light source at 450 nm and a distance of 0.2 meters will also create a sharp image of a 550 nm light source more than 4 meters away. All of these distances scale with the diameter of the lens, in this case 10mm.

We assert that our model is consistent with existing data on both cephalopod retinal morphology and behavior. Two lines of evidence drove (5) the prevailing view that cephalopods are color blind. First, numerous studies show (2,3,4) that only one photoreceptor type exists in the cephalopod retina. Our mechanism for color discrimination requires only one receptor type. Second, a suite of behavioral experiments designed to test for opponent color vision in cephalopods suggest that it is not present. With our proposed mechanism cephalopods cannot resolve (Fig. 3) an edge between two abutting colors of comparable intensity. This explains why optomotor assays and camouflage using abutting colors (5,21,22) (such as the yellow/green checkerboard experiment) return a null result. Similarly, experiments with monochromatic light projected (23) onto a large uniform reflector or training experiments with rapidly vibrating colored cues (20,21) would defeat a determination of chromatic defocus. We believe the fact that cephalopods fail these specific experimental challenges yet succeed at matching more complex natural backgrounds constitutes strong behavioral evidence for our model.

The spectral discrimination mechanism proposed here is amenable to appropriately designed laboratory tests, using sharp transitions between black patterns on a variety of colored backgrounds to evaluate camouflage effectiveness. This mechanism also has potential applicability in other species with a limited number of photoreceptor types and a low *f*-number visual system. Some dolphins species utilize (24) an annular pupil, a similar (25) graded index of refraction lens, and display some evidence for behavioral color discrimination (26) in regimes where their visual system would have difficulty (27) encoding color by opponent channels. A large number of species that are active both diurnally and nocturnally possess (28) an annular pupil and we wonder if these organisms could also benefit from color discrimination by this mechanism.

Another interesting circumstance involves the detection and characterization of spectrally variable bio-luminescent point sources. Deep sea squid and octopus have a fast visual system that should allow these animals to use the shape of the point spread function of unresolved sources (at a fixed accommodation setting) to deduce the spectrum of the detected light, allowing them to not only detect light-emitting animals but also discriminate between their unique spectral signatures.

METHODS

Chromatic Aberration Computation - Using measured (16) optical properties of *Octopus australis* we performed a simulation by constructing a hyperspectral image cube (at 5 microns per pixel, corresponding to a cephalopod rhabdome diameter (ref), and 200 planes spanning $450 < \lambda < 650$ nm in the spectral direction at $\Delta\lambda$=1 nm). We modeled an *f*/1.2 spherical lens with a diameter of 10 mm, but our computed chromatic blurring results are independent of this choice of scale. For each lens-to-retina focal distance, which brings a single wavelength into crisp focus, we computed the pupil-dependent chromatic image blur at the other wavelengths. We then summed up the image cube along the wavelength direction, weighted by seawater-filtered solar photon illumination times the opsin response curve (Extended Data Fig. 1), to arrive at a final simulated chromatically blurred image on the retina. This is repeated for a sequence of accommodation values, for three different pupil shapes. We computed a Modulation Transfer Function (MTF, Fig. 3) metric, to map out image acuity as a function of accommodation, pupil shape, and the spectral content of the test image.

The chromatic aberration shown in Fig. 3 of the paper was computed with a MATLAB code, chromatic.m, that was adapted from a program initially written by C.W.S. to investigate the out-of-focus properties of the Large Synoptic Survey Telescope (LSST). The encircled energy diagrams shown below were computed with a related program, PSF.m. (will be posted upon publication)

We computed the image formed on the retinal surface for a number of bar chart test patterns, as seen through a variety of pupils, for a detected-photon spectrum that is representative of a visually rich marine environment.

The detected light intensity I(i,j) in each pixel (i,j) of the simulated retinal image is given by

$$I(i,j) = \int_{\lambda_1}^{\lambda_2} \Phi_{solar}(\lambda) e^{-D/z(\lambda)} R(i,j,\lambda) OTF(i,j,\lambda) d\lambda$$

where F_{solar} is the solar photon irradiance, the exponential term accounts for the reduction in down-welling photon flux at a water depth D with an attenuation length $z(\lambda)$, $R(i,j,\lambda)$ is the spectral reflectance of the portion of the scene imaged by pixel (i, j), and OTF is the optical transfer function of the visual system, including both aberration effects and the spectral sensitivity of the photoreceptor opsin. The limits of integration span the spectral range of interest, in this case band-limited by the opsin response.

Illumination - We used a ground-level spectrum of solar irradiance from http://www.pvlighthouse.com.au/resources/optics/spectrum%20library/spectrum%20library.aspx, multiplied by λ to convert to relative photon irradiance. To account for illumination attenuation at our chosen nominal depth of D=3 meters we used the Pacific seawater optical attenuation length data (29). We used the attenuation lengths

appropriate for depths of 0-20 meters, which correspond to a chlorophyll density of 0.043 mg m^{-3}. The resulting photon irradiance spectrum is presented in Extended Data Fig. 1. The depth is a free parameter in our code and other depth choices do not change the basic result presented in the paper.

Reflectance Spectra and Test Images - Each pixel in the simulated test image was assigned a reflectance spectrum that was a weighted superposition of three template reflectance spectra. To simulate the colors encountered in marine settings we drew our three Eignespectra from typical biologically derived marine spectra measured (19) from reflectance spectroscopy in the field.

These are also shown in Extended Data Fig. 1. Since the opsin response is effectively zero for the reddest of these spectra, only the two bluer components made a significant contribution to I(i,j). We produced a variety of dual-color bar charts with varying spatial frequency in order to assess the acuity of the resulting images. The spatial scale of these test images was set to 5 microns per pixel, which corresponds to the typical diameter of the photosensitive structures (rhabdomes) that pave the retinal surface of cephalopods. We produced bar chart test patterns with bright bar widths ranging from 112 pixels to 2 pixels. At our sampling of 5 microns per pixel this corresponds to 165 micron and 10 micron widths, respectively, on the retina.

Optical Transfer Function (OTF) – The imaging properties of the cephalopod visual system are determined by the combination of the pupil shape, the refractive properties and configuration of the optical components, and the shape and location of the retinal surface. Rays first propagate through the pupil, which determines both the collecting area and the off-axis distances, *h*, of the rays that are imaged onto the retinal surface. The cephalopod lens is well-approximated by a sphere with a radial gradient in the index of refraction that produces a remarkably effective correction for spherical aberration (16). But the wavelength-dependence of the index of refraction does produce chromatic aberration. Rays of different wavelengths therefore have different effective focal lengths. The blur induced by this chromatic focal length variation depends on the angle at which the rays intersect the optical axis, which in turn scales with the ray's distance off-axis. Pupils that transmit a large proportion of off-axis rays therefore produce more chromatic blurring than pupils that are predominantly on-axis.

When chromatically out-of-focus rays of a given wavelength intersect the retina, they have a point spread function that is an image of the pupil. The resulting focal plane image at each wavelength is a convolution of this point spread function with the test pattern image. We computed this convolution for a discrete set of wavelengths, and summed the resulting hyperspectral synthetic image along the spectral direction to arrive at a final full-spectrum simulated image.

We produced three different planar pupil masks. One corresponds to the full useful aperture of the lens, with a pupil diameter of 8 mm. The second mask is an axially-centered pupil with a diameter of 1mm, the size at which diffraction and chromatic effects are comparable. The third pupil approximates the U-shaped annular component seen in many free-swimming diurnal cephalopods under bright illumination (shallow water squid and cuttlefish), with an inner diameter of 6 mm, an

outer diameter of 6.66 mm, and a polar angle extent of 180 degrees, oriented to be reflection-symmetric about a vertical axis.

Our MATLAB program uses the wavelength-dependence of the focal length of the *Octopus australis* eye as reported (16) by Jagger and Sands. Their laboratory measurements show a sub-percent perturbation in focal length due to residual spherical aberration, but a chromatic fractional shift in focal length, d*f*/*f*, of 4.1% between 450 and 700 nm. A second-order polynomial fit to the data in Jagger & Sands yielded $df/f = -5.4676 \times 10^{-5} \lambda^2 + 0.0794 \lambda - 27.1047$, with $df/f=0$ at 550 nm.

We modeled a cephalopod lens with a diameter of d=10 mm and a focal length of f=12 mm at 550 nm. The spectral range used in the computer model was restricted to $450 \text{ nm} < \lambda < 650 \text{ nm}$ in order to avoid making an extrapolation from the measured chromatic focal changes reported by Jagger & Sands. If we chose to extrapolate beyond this range of wavelengths this would only strengthen our result. Substantial amounts of illumination (15% of the photons) lie between 350 and 450 nm, and the chromatic focus perturbations are enhanced at short wavelengths, so for our point spread function estimates (presented below) we do extrapolate the Jagger and Sands data down to 350 nm, using the expression given above, in conjunction with the attenuated photon spectrum and the opsin response. The opsin photon sensitivity curve we used was from Chung (4).

Our image simulation program used an outermost loop that stepped through a sequence of best-focus wavelengths. This amounts to successively changing the lens-to-retina separation, bringing light of different wavelengths to best-focus at different spacings. For each accommodation value (*i.e*. lens-to-retina separation) we then iterated through illumination wavelengths and computed the appropriate focus offset and blur for that wavelength. The sum, in the wavelength direction, of the blurred hyperspectral image stack produced a 2-d simulation of the test pattern image on the retina, integrated over illumination wavelengths and the opsin response function, for $450 < \lambda < 650$ nm. We took care to introduce appropriate parity flips of the annular pupil according to the sign of the focal length offset at each wavelength. The summed images were normalized so that the flux value in a resolved test bar was unity.

Modulation Transfer Function (MTF) Analysis – The wavelength-integrated blurred test pattern images were each analyzed to assess the sharpness of the image, using line profile plots across the images. We defined an MTF metric that has the merit of being simple; we computed two times the standard deviation of the pixel values in each image. A crisp image has a bimodal intensity histogram (predominantly 1's and 0's) and a high standard deviation. A highly blurred image has an intensity histogram peaked at the mean pixel value, and a low standard deviation. By mapping out this MTF metric vs. lens-to-retina spacing, we can quantitatively assess the extent to which image sharpness can be used to deduce scene spectral content. These results are presented as MTF vs. accommodation plots, for various pupil shapes and simulated scene spectral content.

Image Quality Budget - We evaluated the various terms in the image quality budget, shown in Supplementary Table 1, using geometrical or diffractive optics

principles, as appropriate. Each entry in Supplementary Table 1 is provided as Gaussian-equivalent FWHM in the focal plane, in units of microns, for the $f/1.2$ spherical lens and a 12 mm focal length, with a radial gradient in index of refraction that compensates for spherical aberration. The individual entries in the table are based on the reasoning presented below. We also note the dependencies on pupil geometry and wavelength for the various contributions to image blurring. For pupil sizes larger than 1 mm diameter, chromatic aberration dominates the image quality budget.

Photoreceptor size. The typical diameter for the rhabdomes tiled across the cephalopod retina is reported (14) to be 5 microns. This sets a limit on spatial sampling in the focal plane. The propagation of light rays across adjacent rhabdomes (1) ("rhabdome crosstalk") would induce additional (and potentially chromatic) image degradation, but studies of cuttlefish retina concluded (30, 31) that their rhabdomes are clad in pigmented sheathing that may suppress this potential source of image degradation. We therefore elected to not include any potential image degradation from rhabdome crosstalk. We note that if rhabdome crosstalk were a significant contributor to image blur this would not favor the annular pupil shape seen in these animals.

Retinal displacement. Cross sectional light micrograph images of cephalopod retinal structure indicate (31) an rms axial displacement of at most a few microns over spatial scales of tens of microns. This translates into a defocus blur of order 1 micron for the full-aperture pupil. The retinal displacement would have to be comparable to the chromatic focus shift (of order 100 microns) in order to produce image degradation comparable to the chromatic blur. (We do note the "retinal bump" in cephalopods could provide spectral information at fixed accommodation if the line of sight is varied (32) so as to shift the scene across this perturbation in effective focal length or if the object of interest's image on the retina spans the retinal bump.)

Residual spherical aberration. Although a spherical lens of uniform index of refraction produces pronounced spherical aberration, numerous studies have shown that the lenses of fishes and cephalopods have a radial variation in index of refraction that largely compensates for spherical aberration. Jagger & Sands show a typical FWHM from on-axis residual spherical aberration in octopus of less than 5 microns (16) at full aperture. That was for lenses a factor of two smaller than our 12 mm focal length model, so we have scaled this up to 10 microns for the entry in the image quality budget. We note also that this is for full-aperture imaging, and that the annular pupil greatly reduces the radial span of rays in the system, so this is a conservative overestimate for that pupil geometry.

Chromatic Aberration. Wavelength-dependence of the index of refraction within the lens induces wavelength-dependent defocus at the retina. The experimental data (16) clearly indicate a wavelength-dependent focal shift in the lens of the octopus. We used our quadratic fit to the fractional chromatic focal length shift measured for octopus lenses from Jagger & Sands to perform a numerical computation of the 80% encircled energy radius for a point source at infinity, with best-focus accommodations

corresponding to wavelengths between 350 and 650 nm, for the three different pupil geometries we studied. For this computation we were interested in the entire wavelength range of interest, and so we extended the focal length dependence on wavelength fit down to wavelengths of 350 nm. The encircled energy as a function of distance from the centroid is shown in Extended Data Fig. 3. We converted from the 80% encircled energy radius, R80, to a Gaussian-equivalent FWHM = R80 x 1.3. This produced FWHM Gaussian equivalents of 6, 48 and 61 microns for the small, full and annular pupils, respectively, at the best-focus wavelength of 500 nm, the peak of the opsin curve.

Diffraction. The diffraction limit on the focal plane has a spatial FWHM given by $FWHM_{diff} = f/\# \lambda$. For our full-pupil with d = 8 mm, at the wavelength of peak opsin sensitivity this gives $FWHM_{diff}$ = 1.5 x 0.5 microns = 0.75 microns. Stopping down the pupil to a smaller diameter d increases this term by a multiplicative factor of (8 mm/d). Our smallest circular pupil diameter of d=1 mm produces a diffraction limit of 6 microns FWHM, which is equal to the chromatic aberration term.

Pupil-Dependence of the Spectral Resolution – A quantitative assessment of the pupil-shape dependence of spectral sensitivity (Extended Data Fig. 2) bears out the qualitative argument made above. The small axial pupil produces an image with an MTF that is largely insensitive to accommodation, due to the increased depth of focus. The annular and full-aperture pupils have superior and very similar spectral resolution. This comparison was performed with the Black-Yellow test pattern.

Color-Range Ambiguity – If spectral information is obtained by making a differential comparison of image sharpness vs. accommodation, there is a potential ambiguity between range and spectral content. A blue disk against a dark background might have the same sharpest-image accommodation setting as a redder disk that is farther away. We contend that this degeneracy can be resolved in three ways: (1) if a foreground object has spectral diversity at high spatial frequency, the *relative* spectral content of pixels against a darker background can be determined, (2) if the object is sufficiently far away, there is no range-color degeneracy, and (3) an independent determination of distance, using binocular vision or some other means of distance determination, will break the degeneracy. We computed the accommodation needed to achieve a focused image as a function of both object distance and wavelength, at λ=450, 500 and 550 nm. These wavelengths correspond to the opsin peak and the 50% sensitivity points on either side. Extended Data Fig. 4 shows that unambiguous spectral discrimination can be achieved for objects at distances beyond 0.75 meters, for a 10 mm diameter lens. The spherical lens system obeys an implicit equation for the accommodation distance I, as a function of lens focal length *f* and object distance O, that is a modified version of the lensmaker's equation for thin lenses, given by

$$1 / I = [1 / \cos(a\sin(R / O))](1 / f - 1 / O).$$

References

1. Cronin, T.W., Johnsen, S., Marshall, M.J., Warrant, E.J. *Visual Ecology*. Princeton University Press, Princeton, N.J. (2014).

2. Brown, P. K. and Brown, P. S. Visual pigments of the octopus and cuttlefish. *Nature* **182**, 1288 (1958).

3. Bellingham, J., Morris, A. G., and Hunt, D. M. The rhodopsin gene of the cuttlefish *Sepia officinalis*: Sequence and spectral tuning. *Journal of Experimental Biology* **201**, 2299 (1998).

4. Chung, W. Comparisons of visual capabilities in modern cephalopods from shallow water to deep sea. Univ. of Queensland Ph.D. Dissertation (2014).

5. Mäthger, L. M. *et al*. Color blindness and contrast perception in cuttlefish (Sepia officinalis) determined by a visual sensorimotor assay. *Vision Research* **46.11**, 1746 (2006).

6. Hanlon, R. Cephalopod dynamic camouflage. *Current Biology* **17.11**, R400 (2007).

7. Chiao, C., Chubb, C., and Hanlon, R. T. A review of visual perception mechanisms that regulate rapid adaptive camouflage in cuttlefish. *Journal of Comparative Physiology A*, 1 (2015).

8. Buresch, K. C. *et al*. Cuttlefish adjust body pattern intensity with respect to substrate intensity to aid camouflage, but do not camouflage in extremely low light. *Journal of Experimental Marine Biology and Ecology* **462**, 121 (2015).

9. Akkaynak, D. *et al*. Quantification of cuttlefish (Sepia officinalis) camouflage: a study of color and luminance using in situ spectrometry. *Journal of Comparative Physiology A* **199.3**, 211 (2013).

10. Mäthger, L. M. *et al*. Color matching on natural substrates in cuttlefish, Sepia officinalis. *Journal of Comparative Physiology A* **194.6**, 577 (2008).

11. Hanlon, R. T. *et al*. A fish-eye view of cuttlefish camouflage using in situ spectrometry. *Biological Journal of the Linnean Society* **109.3**, 535 (2013).

12. Chiao, C. *et al*. Hyperspectral imaging of cuttlefish camouflage indicates good color match in the eyes of fish predators. *Proceedings of the National Academy of Sciences,* **201019090** (2011).

13. Kühn, A. Über farbwechsel und farbensinn von cephalopoden. *Zeitschrift für vergleichende Physiologie* 32.6, 572 (1950).

14. Hanlon, R.T. and Messenger, J.B. *Cephalopod Behavior*. Cambridge University Press, Cambridge, U.K. (1998).

15. Mäthger, L. M., Roberts, S. B., and Hanlon, R. T. Evidence for distributed light sensing in the skin of cuttlefish, Sepia officinalis. *Biology letters* **rsbl20100223** (2010).

16. Jagger, W. S., and P. J. Sands. "A wide-angle gradient index optical model of the crystalline lens and eye of the octopus." *Vision research* 39.17 (1999): 2841-2852.

17. Talbot, C. M., and Marshall, J. N. The retinal topography of three species of coleoid cephalopod: significance for perception of polarized light. *Philosophical Transactions of the Royal Society B: Biological Sciences* **366.1565**, 724 (2011).

18. Schaeffel, F., Murphy, C. J., and Howland, H. C. Accommodation in the cuttlefish (Sepia officinalis). *Journal of Experimental Biology* **202.22**, 3127 (1999).

19. Marshall. J. *et al*. Visual biology of Hawaiian reef fishes. III. Environmental light and an integrated approach to the ecology of reef fish vision. Copeia **3**, 467 (2004).

20. Messenger, J. B. Evidence that octopus is colour blind. *Journal of Experimental Biology* **70.1**, 49 (1977).

21. Messenger, J. B., Wilson, A. P., and Hedge, A. Some evidence for colour-blindness in Octopus. *Journal of Experimental Biology* **59.1**, 77 (1973).

22. Marshall, N. J. and Messenger, J. B. Colour-blind camouflage. *Nature* **382**, 408 (1996).

23. Roffe, T. Spectral perception in Octopus: A behavioral study. *Vision Research* **15.3**, 353 (1975).

24. Herman, L. M. *et al*. Bottle-nosed dolphin: double-slit pupil yields equivalent aerial and underwater diurnal acuity. *Science* **189.4203**, 650 (1975).

25. Kröger, R. H. and Kirschfeld, K. Optics of the harbor porpoise eye in water. *JOSA A* **10.7**, 1481 (1993).

26. Griebel, U., and Schmid, A. Spectral sensitivity and color vision in the bottlenose dolphin (*Tursiops truncatus*). *Marine and Freshwater Behaviour and Physiology* **35.3**, 129 (2002)

27. Fasick, J. I. *et al*. The visual pigments of the bottlenose dolphin (Tursiops truncatus). *Visual neuroscience* **15.04**, 643 (1998).

28. Murphy, Christopher J., and Howard C. Howland. "The functional significance of crescent‐shaped pupils and multiple pupillary apertures." *Journal of Experimental Zoology* 256.S5 (1990): 22-28.

29. Morel, A. and Maritonrena, S. Bio-optical properties of oceanic waters: a reappraisal. J. Geophys. Res. **106(CA)**, 7163 (2001).

30. Yamamoto, T., Tasaki, K., Sugawara, Y. and Tonosaki, A. Fine structure of the octopus retina. Journal of Cell Biology **25.2**, 345 (1965).

31. Hao, Z, Zhang, X., Kudo, H. and Kaeriyama, M. Development of the Retina in the Cuttlefish *Sepia esculenta.* Journal of Shellfish Research **29**, 463 (2010)

32. Chung, W. and Marshall, J. Range-finding in squid using retinal deformation and image blur. *Current Biology* **24.2**, R64 (2014).

EXTENDED DATA

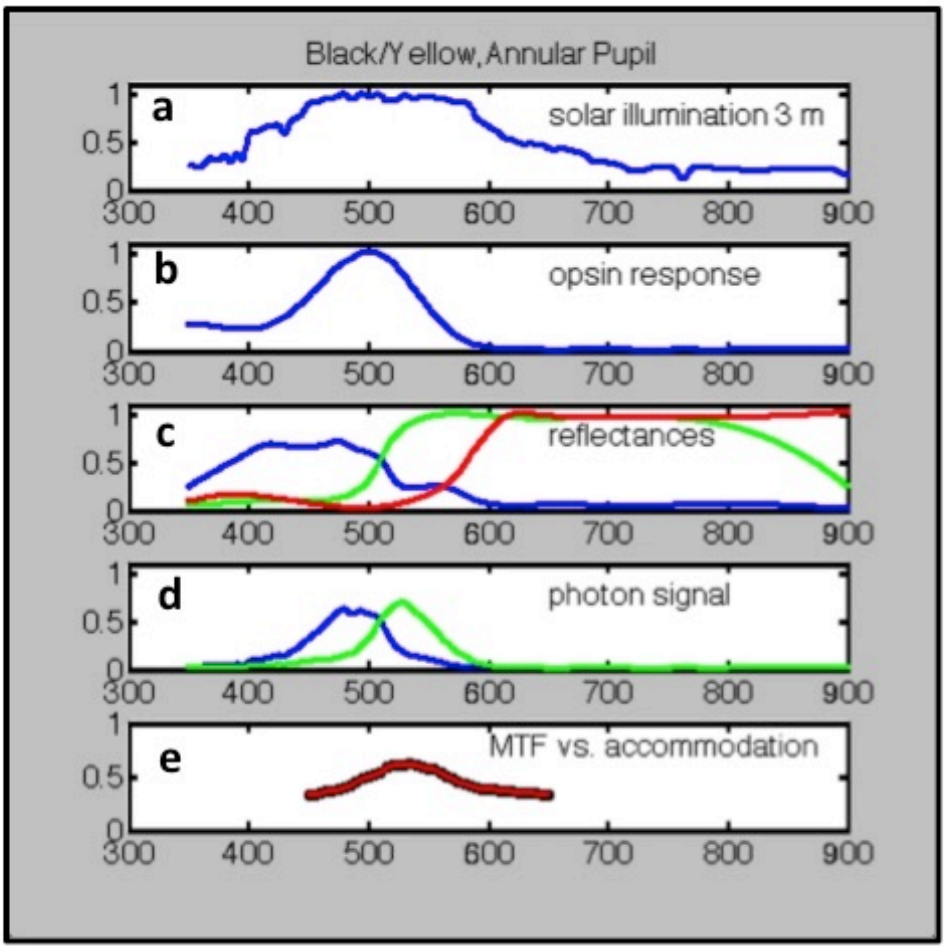

Extended Data Figure 1. This figure shows the wavelength dependence (in nm) of multiple quantities of interest. The depth-attenuated solar photon spectrum is shown in **a.**, the opsin's relative photon sensitivity response function in **b**, the three reflectance eigenspectra we used in **c**, the detected photon flux for the two bluest eigenspectra in **d**, and the measured MTF vs. accommodation for a synthetic test target that alternates bars of Eigenspectrum #2 (shown as the green line) with black bars in **e**.

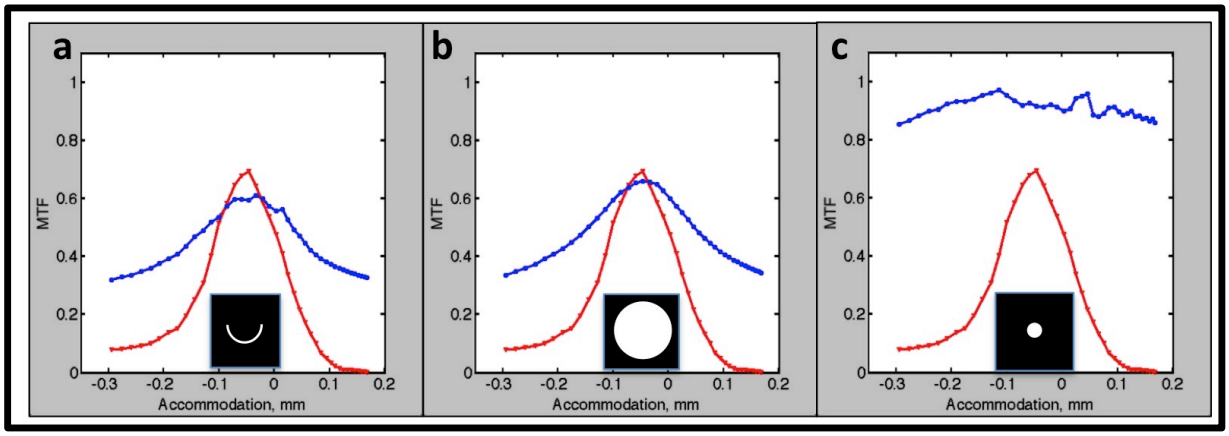

Extended Data Figure 2. **Pupil-dependence of spectral resolution**. These panels show MTF (blue) vs. accommodation for the detectable spectrum shown in red, as a function of pupil size and shape. Panel **a** is the semi-annular pupil with diameter d with 6 mm < d < 6.66 mm, **b** has d = 8 mm, and **c** is a d = 1 mm on-axis pupil. The shallow angle of incidence of the rays through the small axial pupil suppresses chromatic aberration effects. The ragged features are artifacts from aliasing between the out of focus pupil images and the test pattern bars, on various spatial scales.

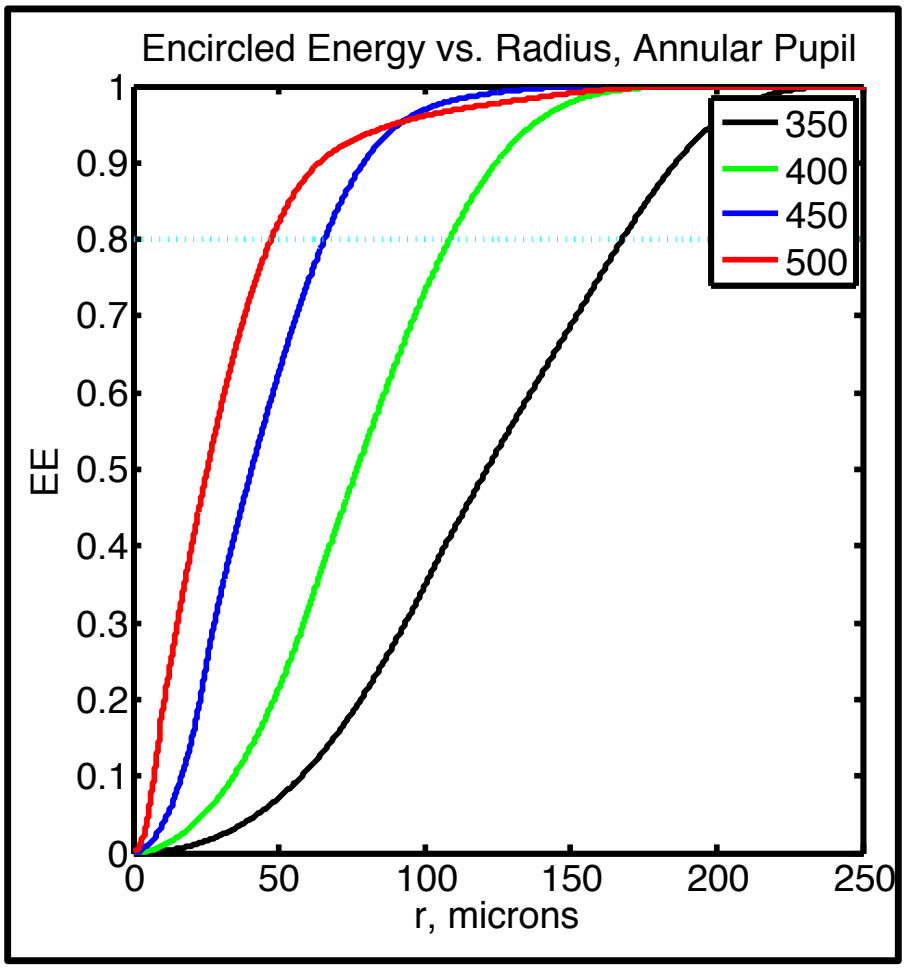

Extended Data Figure 3. **Encircled Energy vs. Radius for various accommodation settings.** This result is for the semi-annular pupil at different accommodation settings indicated as the best-focus wavelength in nm. The plot shows the integrated enclosed energy within the point spread function for the semi-annular pupil geometry. This was computed for a white reflector illuminated by the depth-attenuated solar photon spectrum, for $350 < \lambda < 650$ nm. The red curve yields an 80% encircled energy radius of 47 microns, which corresponds to a Gaussian-PSF-equivalent FWHM of 61 microns, at the accommodation setting of sharpest focus which corresponds to a best-focused wavelength of 500 nm.

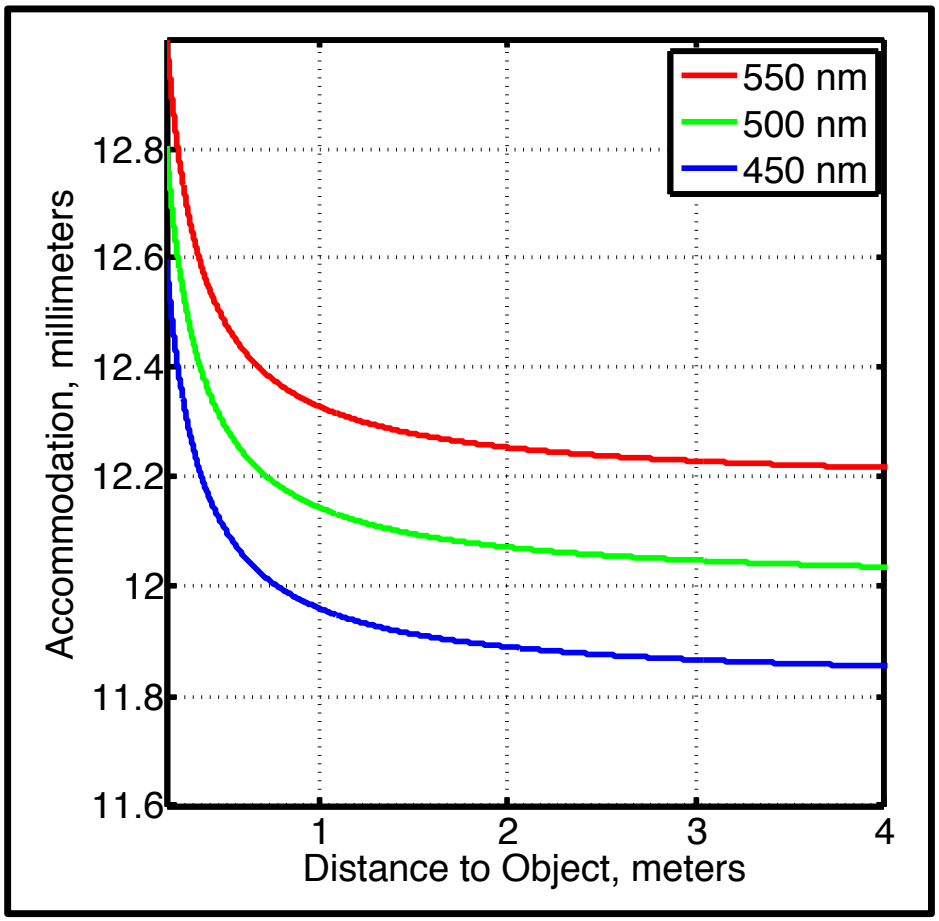

Extended Data Figure 4. Range-color-focus relationship for a 10 mm diameter cephalopod lens. The horizontal axis is the distance to the objects, in meters, and the vertical axis is the accommodation in the optical system, (i.e. the lens-to-retina distance that provides the best focus). The lines show the accommodation vs. range relationship at wavelengths that correspond to the opsin peak (500 nm) and the 50% opsin sensitivity points of 450 nm and 550 nm. Chromatic aberration allows for the unambiguous determination of the color of objects at distances greater than 0.75 meters.

Extended Data Table 1. Cephalopod Retinal Image Quality Budget. The columns present the various aberration phenomena, the resulting Gaussian-PSF equivalent FWHM, and the dependencies on ray height h and on wavelength λ. Note that chromatic aberration is by far the dominant contribution to image blurring, down to pupil diameters of 1 mm.

Term	FWHM (microns)	h-dependence	λ-dependence
Photoreceptor size	5	none	none
Retinal surface displacement	1	$\propto h$	none
Crosstalk between photoreceptors	Neglected (see text)	$\propto h$	unknown
Residual Spherical aberration	10	$\propto \Delta h$ for annular pupil	none
Diffraction d=8 mm on-axis pupil d=1 mm on-axis pupil	 0.75 6	$\propto h^{-1}$	$\propto \lambda$
Wavefront error	unknown	-	-
Chromatic Aberration: d=1 mm, on-axis pupil d=8 mm, on-axis pupil semi-annular pupil	 6 48 61	$\propto h$	none

Acknowledgments: A.L.S. thanks UC Berkeley and the Museum of Vertebrate Zoology for their support, and is grateful to Professor J. McGuire for extensive opportunities and mentoring, and R. Caldwell, and M. Banks for conversations. C.W.S. acknowledges the support of Harvard University. We also thank E. Carrington Gregory for comments and editorial support. The photographs in Fig. 1 were provided by Klaus Stiefel (**a**) and Lakshmi Sawitri (**b,c,d**), under the Creative Commons license.

Author Contributions: A.L.S. proposed chromatic aberration as a potential mechanism for color discrimination in monochromatic visual systems, recognized that previous demonstrations of colorblindness in cephalopods would fail to detect this sensory modality, and considered the biological adaptations associated with this mechanism. C.W.S. performed the computational modeling of chromatic optical systems, and generated the associated figures. Both authors contributed equally to the writing of the manuscript.

Author Information: Requests for further information should be sent to astubbs@berkeley.edu. The authors declare no competing financial interests.